J. Fluid Mech. (2019), *vol.* 862, R2, doi:10.1017/jfm.2018.971

JFM RAPIDS
journals.cambridge.org/rapids

The onset of transient turbulence in minimal plane Couette flow

Julius Rhoan T. Lustro[1], Genta Kawahara[1,†], Lennaert van Veen[2], Masaki Shimizu[1] and Hiroshi Kokubu[3]

[1]Graduate School of Engineering Science, Osaka University, 1-3 Machikaneyama, Toyonaka, Osaka 560-8531, Japan

[2]Faculty of Science, University of Ontario Institute of Technology, 2000 Simcoe Street North, Oshawa, Ontario L1H 7K4, Canada

[3]Graduate School of Science, Kyoto University, Kitashirakawa Oiwake, Sakyo, Kyoto 606-8502, Japan

(Received 16 May 2018; revised 17 November 2018; accepted 27 November 2018; first published online 10 January 2019)

The onset of transient turbulence in minimal plane Couette flow has been identified theoretically as homoclinic tangency with respect to a simple edge state for the Navier–Stokes equation, i.e., the gentle periodic orbit (the lower branch of a saddle-node pair) found by Kawahara & Kida (*J. Fluid Mech.*, vol. 449, 2001, pp. 291–300). The first tangency of a pair of distinct homoclinic orbits to this periodic edge state has been discovered at Reynolds number $Re \equiv Uh/\nu = Re_T \approx 240.88$ (U, h, and ν being half the difference of the two wall velocities, half the wall separation, and the kinematic viscosity of fluid, respectively). At $Re > Re_T$ a Smale horseshoe appears on the Poincaré section through transversal homoclinic points to generate a transient chaos that eventually relaminarises. In numerical experiments a sustaining chaos, which is a consequence of period-doubling cascade stemming from the upper branch of another saddle-node pair of periodic orbits, is observed in a narrow range of the Reynolds number, $Re \approx 240.40$–240.46. At the upper edge of this Re range it is found that the chaotic set touches the lower branch of this pair, i.e., another edge state. The corresponding chaotic attractor is replaced by a chaotic saddle at $Re \approx 240.46$, and subsequently this saddle touches the gentle periodic edge state on the boundary of the laminar basin at the tangency Reynolds number $Re = Re_T$. After this crisis on the boundary of the laminar basin, for $Re > Re_T$, chaotic transients that eventually relaminarise can be observed.

Key words: chaos, transition to turbulence

† Email address for correspondence: kawahara@me.es.osaka-u.ac.jp

1. Introduction

One of the long-standing problems in fluid mechanics is the phenomenon of transition to turbulence (Reynolds 1883). Specifically, in flows at the Reynolds number below its critical value of linear stability, experiments and numerical studies have demonstrated that a finite-amplitude disturbance can trigger the transition. In this case of subcritical transition, turbulence first appears as local patches bounded by laminar flow when a threshold perturbation is crossed. Such localised turbulence is transient in nature and is commonly observed in wall-bounded shear flows, such as boundary layer, plane Poiseuille flow, plane Couette flow, circular-pipe flow and square-duct flow.

In the last two decades researchers have found success in applying dynamical systems theory in elucidating subcritical transition to turbulence (Kerswell 2005; Eckhardt *et al.* 2007, 2008; Kawahara, Uhlmann & van Veen 2012). The dynamical systems approach interprets the transitional flow as a system being regulated by invariant sets in phase space. Invariant sets or solutions have the property that any state point within them will have its trajectory remain within the set forwards and backwards in time. In this context, the transition to turbulence in shear flows corresponds to the coexistence of two invariant sets. One is stable and corresponds to laminar flow. The other may be stable or marginally unstable and corresponds to chaotic motion. Each of these sets has a basin of attraction, i.e., a set of initial conditions that it attracts. These laminar and chaotic basins meet along a border called the 'edge of chaos' (Skufca, Yorke & Eckhardt 2006; Schneider *et al.* 2008; Vollmer, Schneider & Eckhardt 2009; Muñoz *et al.* 2012; Chian, Muñoz & Rempel 2013). A particularly interesting situation occurs if this edge is formed, at least locally, by the stable manifold of a saddle-type invariant solution, which is then called an 'edge state' (Skufca *et al.* 2006; Schneider *et al.* 2008). Edge states have been computed in various shear flows, and it has been demonstrated that they can be ingredients in flow control (see Kawahara 2005).

We focus on the invariant time-periodic solution in minimal plane Couette flow (Kawahara & Kida 2001; Kawahara 2005). This so-called gentle periodic orbit (GPO), which arises as the lower branch from a saddle-node bifurcation, has only one unstable direction and is an edge state in this system. A previous work on this system, which is the motivation of our study, identified homoclinic orbits to this GPO at a relatively high Reynolds number $Re = 400$ (van Veen & Kawahara 2011). These homoclinic orbits are sets of points that converge to the GPO both forward and backward in time. Such presence of homoclinic orbits to the GPO suggests transversal intersections of unstable and stable manifolds (see figure 1), which then implies the existence of a Smale horseshoe generating chaos (Guckenheimer & Holmes 1983; Palis & Takens 1993; Ott 2002). Thus, we would like to stress that the computation of orbits homoclinic to the GPO in this study provides a connection between the theoretical determination of transient turbulence and a classical result from chaos theory. Here, we explore the first appearance of homoclinic orbits at what is called a homoclinic tangency, i.e., tangent homoclinic orbits (see figure 2 for a schematic illustration), at a much smaller Reynolds number and show that this tangency marks the onset of transient turbulence that eventually relaminarises.

For identifying the tangency, we use a method inspired by the work of Itano & Toh (2001), which is related to the edge-tracking algorithm described by Skufca *et al.* (2006) and Schneider *et al.* (2008). This method relies on the fact that the GPO has only a single unstable direction, so that homoclinic points in its unstable

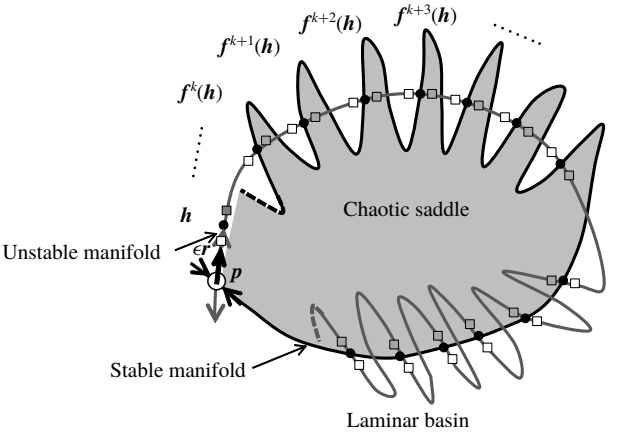

FIGURE 1. The unstable and stable manifolds of the GPO and the homoclinic points $\boldsymbol{h}$ and $\boldsymbol{f}^n(\boldsymbol{h})$ $(n = 1, 2, \ldots)$ on the Poincaré section Σ. The Poincaré section has an intersection at $\boldsymbol{p}$ with the GPO. The boundary of the shaded chaotic basin is formed by the GPO and its stable manifold. A homoclinic point $\boldsymbol{h}$ is supposed to be close to $\boldsymbol{p}$. The nth iterate of the Poincaré map is denoted by $\boldsymbol{f}^n$. The unstable and stable manifolds are shown, respectively, by the grey and black curves, and the homoclinic points are represented by black dots. The unstable eigenvector $\boldsymbol{r}$ is tangent to the unstable manifold of the GPO at $\boldsymbol{p}$. The squares stand for the sequence of mapped points $\boldsymbol{f}^n(\boldsymbol{p} + \epsilon\boldsymbol{r})$ $(n = 1, 2, \ldots)$, where ϵ is a positive small parameter. For the case of ϵ just below (or above) $\|\boldsymbol{h} - \boldsymbol{p}\|/\|\boldsymbol{r}\|$ the mapped points are represented by white (or grey) symbols.

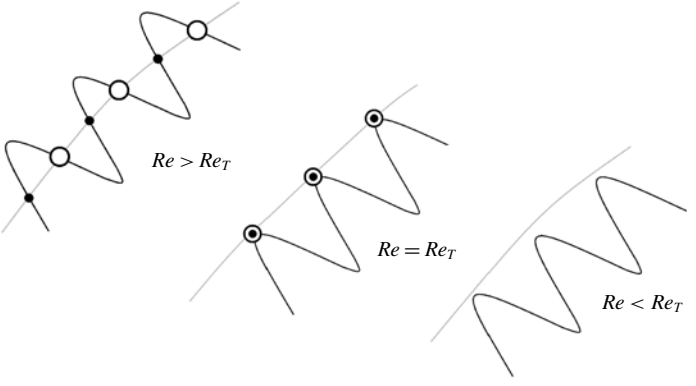

FIGURE 2. Schematic illustration of homoclinic tangency in the Poincaré section. Grey and black lines represent unstable and stable manifolds of the GPO, respectively. Open and closed circles represent two distinct series of homoclinic points, i.e., intersections of two distinct homoclinic orbits. For $Re > Re_T$, transversal homoclinic points appear on the transversal intersections of unstable and stable manifolds of the GPO. At $Re = Re_T$, homoclinic points start to appear due to tangency of unstable and stable manifolds of the GPO. For $Re < Re_T$, homoclinic points do not exist because there is no intersection of unstable and stable manifolds of the GPO.

manifold can be selected by tuning a single parameter. In the more general case of multiple unstable directions, a more computationally demanding boundary value problem, which includes the adjoint linear equations, must be solved (Doedel *et al.* 2009).

In this study, we provide a theoretical description of the onset of transient turbulence in minimal plane Couette flow through the identification of the first homoclinic tangency to the edge state GPO. In incompressible Keplerian shear flow, Riols *et al.* (2013) have reported the possible role of homoclinic and heteroclinic tangles in their numerical experiments leading to chaotic dynamics, but to the authors' knowledge, the onset of such transient turbulence has yet to be described theoretically. We numerically compute homoclinic orbits to the GPO and track them down with decreasing Reynolds number to identify their onset as tangency. The search leads to a few pairs of distinct homoclinic orbits in which the two homoclinic orbits move closer to each other as the Reynolds number decreases, and eventually collide and disappear at a tangency Reynolds number (see figure 2). Grebogi, Ott & Yorke (1983) first identified homoclinic tangency in the Hénon map as a mechanism that causes boundary crisis, i.e., the sudden disappearance of a sustaining chaotic set as it touches a periodic edge state at the critical parameter. In this work we also confirm the relevance of the theoretical determination of the onset Reynolds number of transient turbulence to the numerically observed boundary crisis Reynolds number.

2. Flow configuration and numerical computations

We consider plane Couette flow, i.e., the viscous flow between two moving parallel plates which have a no-slip and impermeable surface and are separated by a distance $2h$. Let x, y and z denote the streamwise, the wall-normal and the spanwise coordinates, respectively, and let their origin be on the midplane. The upper (or lower) plate at $y/h = +1$ (or -1) moves in the positive (or negative) x-direction at a constant speed U. The Reynolds number is defined as $Re = Uh/\nu$, where ν is the kinematic viscosity of fluid. Spatial periodicity is imposed on the flow in the x- and z-directions. The streamwise and spanwise periods are set to the minimal dimensions $(L_x/h, L_z/h) = (1.755\pi, 1.2\pi)$ for sustaining turbulence (Kawahara & Kida 2001), i.e., the minimal flow unit first introduced by Jiménez & Moin (1991) and Hamilton, Kim & Waleffe (1995). Although plane Couette flow in a larger periodic domain is closer to real flow in an experiment or to ideal flow in a theory, such an extended system is far beyond a dynamical systems approach to be taken in this paper. Therefore, as the first step to understanding the onset of transient turbulence, we investigate the minimal flow to characterise its onset in terms of a dynamical systems theory. Note that in the minimal flow unit, the Nagata (1990) steady solution, i.e., an edge state, does not exist, at least at a low Reynolds number (see Jiménez *et al.* 2005). Instead, the edge state in this flow is a time-periodic variation, which shows weak, meandering streamwise streaks (Kawahara & Kida 2001; Kawahara 2005). This GPO has a single unstable Floquet multiplier and thus its unstable manifold is two-dimensional and its stable manifold has codimension one in phase space (Kawahara 2005). Both the GPO and its unstable manifold are contained in a subspace invariant under the spatial symmetries given by reflection in the midplane, followed by a streamwise shift over $L_x/2$, and reflection in the streamwise and spanwise directions, followed by a spanwise shift over $L_z/2$ (Kawahara & Kida 2001).

The incompressible Navier–Stokes equation is numerically solved by using a spectral method. The scheme for the numerical solution is essentially the same as

that used by Kim, Moin & Moser (1987), i.e., Crank–Nicolson for the viscous terms and Adams–Bashforth for the nonlinear terms. The streamwise volume flux and the spanwise mean pressure gradient are respectively set to zero. Dealiased Fourier expansions are employed in the x- and z-directions, and Chebyshev-polynomial expansion in the y-direction. In the representation of a GPO and an eigensolution thereof in phase space, modified Chebyshev polynomials are used instead of the original Chebyshev polynomial to satisfy boundary conditions on the walls (see McFadden, Murray & Boisvert 1990). Numerical computations are carried out on 33 792 ($=32\times33\times32$ in x, y and z) grid points for the Reynolds number $Re\leqslant520$. It is confirmed that the behaviour of the numerical solution is qualitatively the same as that for the lower resolution ($16\times33\times16$).

We compute the GPO using the Newton–GMRES (generalised minimal residual) method and examine stability of the computed GPO to infinitesimal disturbances with the same periodicities by using the Arnoldi iteration. These numerical procedures employ the above-mentioned time-stepping computation, and are basically the same as that proposed by Sánchez *et al.* (2004) and Viswanath (2007). In the Newton–GMRES computation a GPO and its period T are numerically obtained for a fixed phase of the periodic orbit. The eigenvalues (Floquet multipliers) and the corresponding eigenvectors of the monodromy matrix with respect to the GPO are then computed numerically.

Homoclinic orbits are tracked down by use of ordinary time-marching of an initial point for $Re\leqslant260$. Take note that the arclength continuation method (van Veen, Kawahara & Matsumura 2011) which was used by van Veen & Kawahara (2011) to extract homoclinic orbits at $Re=400$ is not used at much lower Re in this study. Instead, a bisection method, which is similar to the one used by Itano & Toh (2001), Skufca *et al.* (2006) and Schneider *et al.* (2008) for simple invariant solutions, is used for the numerical computation of a homoclinic orbit. Let us introduce the Poincaré section Σ such that it can have an intersection at $\boldsymbol{p}$ with the GPO and the (only one) unstable eigenvector $\boldsymbol{r}$ of the Poincaré map can be on it, as shown schematically in figure 1. We anticipate that on the Poincaré section there are transversal intersections, i.e., transversal homoclinic points, between the unstable and the stable manifolds of the GPO at $\boldsymbol{p}$. We suppose that one homoclinic point $\boldsymbol{h}$ is close to $\boldsymbol{p}$. The nth iterate of Poincaré mapping of $\boldsymbol{h}$ yields other homoclinic points $\boldsymbol{f}^n(\boldsymbol{h})$ $(n=1,2,\ldots)$. Let us now consider the initial point on the one-dimensional unstable eigensubspace, which is approximated by $\boldsymbol{p}+\epsilon\boldsymbol{r}$ for a positive small parameter ϵ that is to be determined. This initial point is fed to the time-marching code for the numerical computation of homoclinic orbits. If ϵ is taken to be $\|\boldsymbol{h}-\boldsymbol{p}\|/\|\boldsymbol{r}\|$ such that $\boldsymbol{p}+\epsilon\boldsymbol{r}=\boldsymbol{h}$, this initial point is mapped in time on the sequence of homoclinic points $\boldsymbol{f}^n(\boldsymbol{h})$ $(n=1,2,\ldots)$. If ϵ is just below or above $\|\boldsymbol{h}-\boldsymbol{p}\|/\|\boldsymbol{r}\|$, the mapped points deviate from the corresponding homoclinic points along the unstable manifold, as shown in figure 1. An example of the bisection leading to one homoclinic orbit is shown in figure 3 for $Re=260$, which is not far from the first tangency to be discussed later. In this figure the normalised energy input rate per unit time,

$$I\equiv\frac{1}{2L_xL_z(U/h)}\int_0^{L_x}\int_0^{L_z}\left(\left.\frac{\partial u}{\partial y}\right|_{y=-h}+\left.\frac{\partial u}{\partial y}\right|_{y=+h}\right)\mathrm{d}x\,\mathrm{d}z, \tag{2.1}$$

is depicted as a function of dimensionless time tU/h, where u is the streamwise component of the velocity. I is also regarded as the normalised wall shear rate, and it takes a value of unity in a laminar state. In the case of ϵ just below $\|\boldsymbol{h}-\boldsymbol{p}\|/\|\boldsymbol{r}\|$,

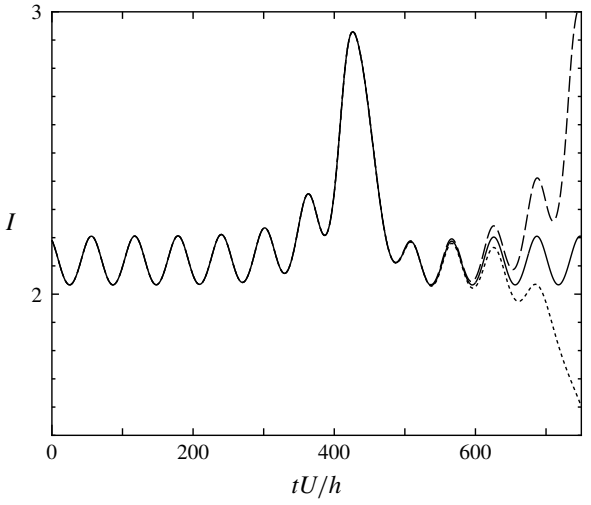

FIGURE 3. The energy input rate I of the three different orbits in the course of bisection as a function of time tU/h at $Re = 260$. Different lines denote initial conditions of different values of ϵ. The solid curve represents a homoclinic orbit, the early and late stages of which exhibit almost-periodic motion. The dotted and dashed curves eventually deviate from the homoclinic orbit to approach a laminar and transiently chaotic state, respectively.

the mapped points are in the laminar basin instead of being on the stable manifold, i.e., the edge of chaos, so that the state point will approach the laminar flow as time goes on (dotted curve in figure 3). On the other hand, in the case of ϵ just above $\|\boldsymbol{h} - \boldsymbol{p}\|/\|\boldsymbol{r}\|$, the mapped points will exhibit (transiently) chaotic behaviour (dashed curve in figure 3). This critically different consequence is a key indicator for one-dimensional bisection as method in searching for a homoclinic orbit with respect to a GPO between laminarisation and transient turbulence. We run a number of initial conditions for different values of ϵ and look for pairs of ϵ that are very close to each other where one goes to laminarisation and the other goes to transient turbulence (dotted and dashed curves, respectively, in figure 3). We expect the ϵ that leads to homoclinic orbit should be in between such pairs since the homoclinic trajectory goes back to the GPO as in the work by van Veen & Kawahara (2011). We use bisection repeatedly on these pairs of ϵ to extract a homoclinic orbit with at least three cycles long of almost-periodic oscillations at the end of the orbit (solid curve in figure 3).

3. Periodic edge states and bifurcation structure

Figure 4 displays a bifurcation diagram of the minimal plane Couette flow showing a value of the local maximum in a time series of I as a function of the Re. This bifurcation diagram closely resembles the one reported by Shimizu *et al.* (2014) for a different physical quantity. The periodic orbit referred to as P1 appears from a saddle-node bifurcation at $Re \approx 236.1$. The lower branch of P1, which is closer to a laminar state for $I = 1$ than the upper branch, is the GPO and is always linearly unstable. Meanwhile, the upper branch is stable to infinitesimal disturbances with the same periodicities as the periodic orbit in the range of $236.1 < Re < 246.2$. In this range, however, the upper branch might become unstable to subharmonic disturbances for a longer streamwise or spanwise period. It is confirmed that the lower branch

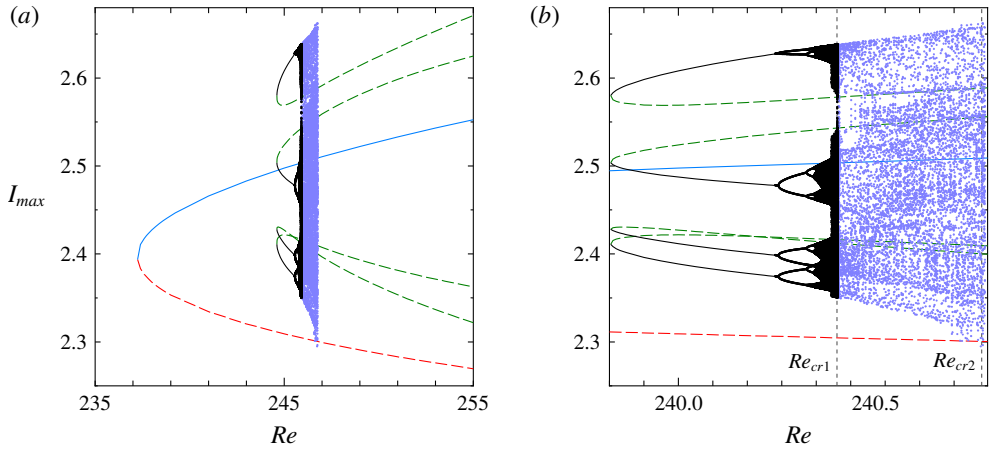

FIGURE 4. The local maximum I_{max} in a time series of energy input at each Reynolds number Re. The right figure shows the magnification of the P2 solution branches and subsequent chaos. The lower (or upper) branch of P1 is coloured red (or blue). The lower branch of P2 (or upper branch of P2 and subsequent period-doubling cascade) is coloured green (or black). The chaotic saddle after the first boundary crisis at $Re = Re_{cr1}$ is coloured violet. In both figures, stable solution branches are represented by solid lines while unstable solution branches are represented by dashed lines. Vertical grey short dashed lines in (*b*) denote the critical Reynolds numbers for the two boundary crises at $Re_{cr1} \approx 240.46$ and $Re_{cr2} \approx 240.88$. At $Re = Re_{cr1}$, the chaotic attractor (black) touches the lower branch of P2 (green). At $Re = Re_{cr2}$, the chaotic saddle (violet) touches the lower branch of P1 (red), i.e., the GPO. It is important to note that these two boundary crises are related to the homoclinic tangencies at the same Re.

has only one real unstable eigenvalue (Floquet multiplier) for the Reynolds number $236.1 < Re \leqslant 520$, as already observed at $Re = 400$ (Kawahara 2005). This implies that in this range of Re the GPO is always an edge state in the minimal flow unit. The upper branch is found to exhibit an oscillatory instability for $Re > 246.2$. A complex conjugate pair of the marginal eigenvalues $\exp(\pm \mathrm{i}\,\theta)$ at $Re \approx 246.2$ has an argument of $\theta \approx 1.85$. Therefore, a torus turns out to arise from this non-resonant bifurcation on the upper branch at $Re \approx 246.2$.

Another periodic orbit referred to as P2 also appears from a saddle-node bifurcation at $Re \approx 239.8$. This orbit (whose I has four local maxima in time) has an unstable lower branch (which is another edge state) and an upper branch that is initially stable. The upper branch of P2 undergoes period-doubling cascade which leads to a chaotic attractor. A boundary crisis between the chaotic attractor and the upper branch of P1 occurs at $Re = Re_{cr1} \approx 240.46$, as observed in an edge state for a laminar basin by Kreilos & Eckhardt (2012) in symmetric plane Couette flow and by Avila *et al.* (2013) in symmetric pipe flow. At this value of Re, the chaotic attractor can touch the lower branch of P2 (see the approaches of the black dots to the green dashed curves in figure 4). As a result, points on the chaotic set can 'leak' to the stable upper branch of P1. The resulting transiently chaotic set is sometimes called a leaky basin. At the Reynolds number above Re_{cr1}, the chaotic attractor is converted to a chaotic saddle and all of the trajectories near it are attracted to the upper branch of P1. Another boundary crisis occurs at $Re = Re_{cr2} \approx 240.88$ (see the approach of the violet dots to the red

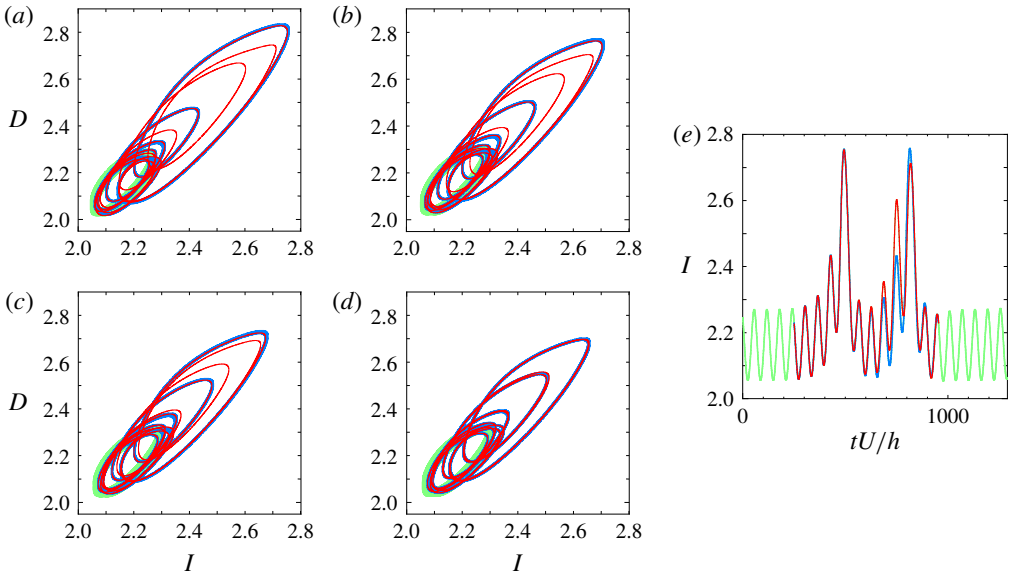

FIGURE 5. A pair of distinct homoclinic orbits to the GPO that exhibit tangency in the (I, D)-projection. The light green line represents the GPO. The blue and red lines correspond to the families of homoclinic orbits referred to as A and B, respectively. Starting from (a) the pair move closer to each other with decreasing Reynolds number until they merge to tangency at (d). The values of Reynolds number from (a) to (d) are: (a) $Re = 245$, (b) $Re = 242.5$, (c) $Re = 241.4$ and (d) $Re \approx 240.88$. The I of the two orbits as a function of time at $Re = 245$ is shown in (e). The blue line is slightly thicker than the red line in order to differentiate one homoclinic orbit from the other, especially during the tangency. A thicker light green line is used to differentiate the GPO from the homoclinic orbits.

dashed curve in figure 4). At this value of the Reynolds number the chaotic saddle touches the GPO. This second crisis creates a leak for state points eventually going to the laminar attractor. Shimizu *et al.* (2014) reported that this chaotic saddle forms a fractal basin boundary between the laminar attractor and P1 (upper branch). The numerically observed formation of the latter leaky basin suggests the first homoclinic tangency to the GPO which can lead to transient turbulence eventually relaminarising and thus will be discussed in the next section.

4. Onset of transient turbulence as homoclinic tangency

In this section we present the discovered orbits homoclinic to the GPO. We search for homoclinic orbits at $Re = 260$ using the method described in § 2 and then track them to the lower Reynolds number. Two-dimensional visualisation of homoclinic orbits is used for simplicity's sake. We encounter several distinct homoclinic orbits during the search and for $Re \leqslant 245$ we confirm the presence of a few pairs in which the two homoclinic orbits move closer to each other with decreasing Reynolds number until they eventually disappear. Figure 5 shows the projection of the two orbits, which have been observed to exist down to the lowest (tangency) Reynolds number, onto a two-dimensional plane of normalised energy input rate I and normalised energy

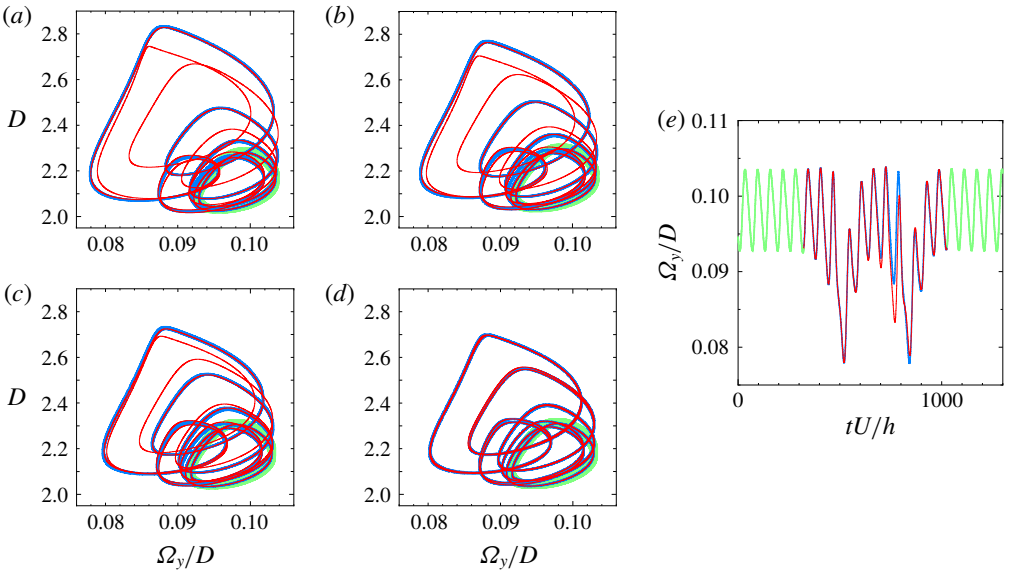

FIGURE 6. The same as figure 5 but for the $(\Omega_y/D, D)$-projection.

dissipation rate per unit time,

$$D \equiv \frac{1}{2L_xL_z(U^2/h)} \int_0^{L_x} \int_{-h}^{+h} \int_0^{L_z} |\boldsymbol{\omega}|^2 \, \mathrm{d}x \, \mathrm{d}y \, \mathrm{d}z, \tag{4.1}$$

$\boldsymbol{\omega}$ being the vorticity vector. Similar to that of I, the value of D in a laminar state is unity. The homoclinic orbits and their tangency are confirmed by projecting them onto another plane, $(\Omega_y/D, D)$, as in figure 6. Here Ω_y is given as

$$\Omega_y \equiv \frac{1}{2L_xL_z(U^2/h)} \int_0^{L_x} \int_{-h}^{+h} \int_0^{L_z} {\omega_y}^2 \, \mathrm{d}x \, \mathrm{d}y \, \mathrm{d}z, \tag{4.2}$$

where ω_y is the wall-normal component of the vorticity. As seen in figures 5 and 6, even at the highest Reynolds number $Re = 245$ the former of the two large-amplitude oscillations (i.e., escape out of the light green GPO) are almost consistent between the two homoclinic orbits while the latter are significantly distinct (see figures 5*e* and 6*e*). As Re is decreased these two homoclinic orbits get closer to each other and eventually merge to disappear in tangency at $Re = Re_T \approx 240.88$. Such merging and subsequent disappearance of the homoclinic orbits suggest the presence of homoclinic tangency, i.e., the origin of a pair of homoclinic orbits, where below the tangency Reynolds number these two orbits cannot exist (see figure 2). The tangency is verified quantitatively by computing the difference of I and D in the close vicinity of $Re = Re_T$ such as

$$d_I = \sqrt{\frac{\displaystyle\int_0^T [I_A(t+\tau) - I_B(t)]^2 \, \mathrm{d}t}{\displaystyle\int_0^T [I_A(t)]^2 \, \mathrm{d}t}}, \quad d_D = \sqrt{\frac{\displaystyle\int_0^T [D_A(t+\tau) - D_B(t)]^2 \, \mathrm{d}t}{\displaystyle\int_0^T [D_A(t)]^2 \, \mathrm{d}t}}, \tag{4.3a,b}$$

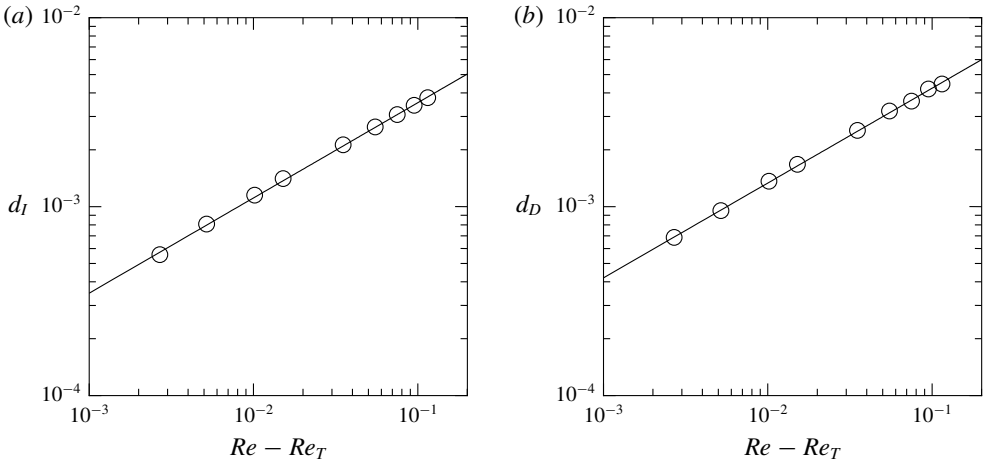

FIGURE 7. Log–log plot of the difference in (*a*) I and (*b*) D between the two homoclinic orbits to the GPO as a function of the increment of the Reynolds number. The lines represent least squares fitting by the function $d = K(Re - Re_T)^{\alpha}$ in the close vicinity of the tangency Reynolds number Re_T. $Re_T \approx 240.88$ and $\alpha \approx 0.50$ in both fittings, while K takes a value of 0.011 and 0.013 for (*a*) and (*b*), respectively.

where the subscripts A and B correspond to the pair of homoclinic orbits and τ denotes the time period shift optimised so that d_I or d_D may be minimal at each Re. Least squares fitting is performed using the equation $d = K(Re - Re_T)^{\alpha}$, where K and α are constants (see figure 7). For both the differences the tangency Reynolds number has been determined as $Re_T \approx 240.88$, and the constant α takes a value almost equal to $1/2$, confirming the multiplicity of the two solutions.

No homoclinic orbits to the GPO have been found below the first tangency Reynolds number Re_T. Dynamical systems theory tells us that the presence of transversal homoclinic orbits (and so transversal homoclinic points on Poincaré section) implies the existence of a Smale horseshoe. The classical Smale–Birkhoff theorem states that transversal crossings of the stable and unstable manifolds in such a Smale horseshoe lead to an intricate tangle of the two manifolds, forming chaotic trajectories in the process (Guckenheimer & Holmes 1983; Palis & Takens 1993; Ott 2002). The transient chaos eventually relaminarising seen in the previous section is observed just above this first homoclinic tangency. Hence, the onset of transient turbulence eventually relaminarising in this system can be explained theoretically in terms of the creation of chaotic orbits as a consequence of this first homoclinic tangency with respect to the GPO for the laminar flow.

5. Relevance of homoclinic tangency to boundary crisis

It is important to emphasise that $Re_T = Re_{cr2} \approx 240.88$, such that the first homoclinic tangency creates the boundary crisis between the upper branch of P1 and the laminar attractor, leading to relaminarisation. Such crisis, which is due to tangency of stable and unstable manifolds, has been demonstrated by Grebogi *et al.* (1983) in the Hénon map. The observed boundary crisis at lower Re, $Re_{cr1} \approx 240.46$, between the upper branch of P1 and the chaotic attractor also implies the existence of homoclinic orbits and their tangency with respect to the lower branch of P2. In reality the first

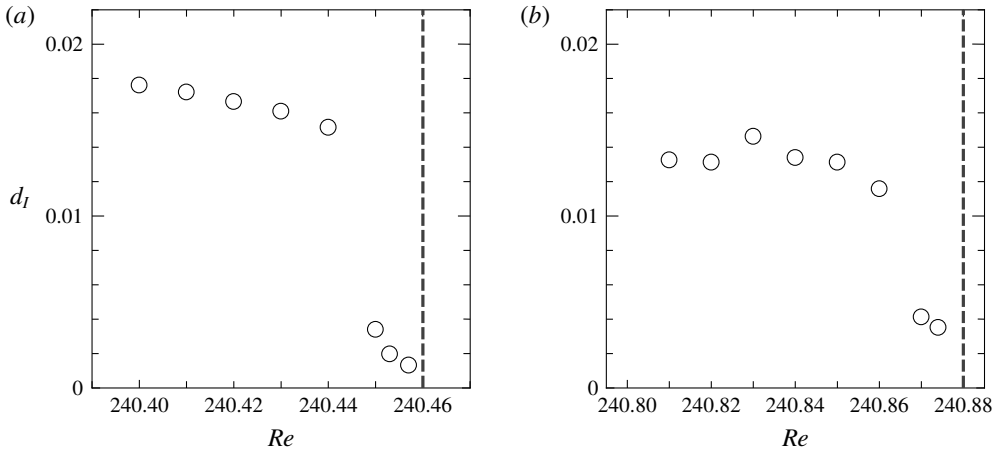

FIGURE 8. (*a*) The difference d_I of the lower branch of P2 from a segment on the chaotic attractor which come closest to the lower branch of P2 just before the first boundary crisis. (*b*) The difference d_I of the GPO from a segment on the chaotic saddle which come closest to the GPO just before the second boundary crisis. Dashed lines represent the corresponding tangency Reynolds numbers.

homoclinic tangency with respect to the lower branch of P2 has also been confirmed at $Re \approx 240.46$ (figure not shown), which is consistent with the crisis Reynolds number Re_{cr1}. We can say that as with the second boundary crisis at $Re_{cr2} \approx 240.88$, the first boundary crisis at $Re_{cr1} \approx 240.46$ is due to the first homoclinic tangency to the lower branch of P2. The approach of the chaotic attractor/saddle to the lower branch of P2/GPO just before the crisis is verified quantitatively by computing d_I introduced in § 4 for a segment of the same period as the lower branch of P2/GPO on the chaotic attractor/saddle which comes closest to the lower branch of P2/GPO. Figure 8 shows the differences of the chaotic segments from the lower branches as a function of the Reynolds number. Although a small discrepancy is still seen because of finite-time numerical observation, significant decreases in the difference d_I can be confirmed just below the tangency Reynolds numbers, as shown in the figures.

For homoclinic orbits to the lower branch of P2 another tangency has also been observed at $Re \approx 240.56$. For homoclinic orbits to the GPO two other tangencies have also been found at $Re \approx 240.89$ and 241.3. One homoclinic orbit in the pair which has tangency at $Re \approx 241.3$ belongs to the family of the homoclinic orbits discovered by van Veen & Kawahara (2011) while the other belongs to a new family found in this study. The two pairs, one of which has the first tangency at $Re = Re_T$ and the other of which has the tangency at $Re \approx 240.89$, all belong to new families. Projection onto both the (I, D) and $(\Omega_y/D, D)$ planes confirms these homoclinic orbits to the lower branch of P2 and GPO as well as their tangency. These homoclinic orbits are paired based on which of them becomes tangent with another one, then the pairs are tracked for increasing Reynolds number. Time evolution of the flow structures along these homoclinic orbits shows a qualitatively similar scenario to the one reported by van Veen & Kawahara (2011), with the streak becoming less deformed during the bursting event because the homoclinic orbit gets closer to the GPO as the Reynolds number is decreased.

The existence of above-mentioned homoclinic orbits to the GPO and the lower branch of P2 suggests presence of heteroclinic orbits. A pair of heteroclinic orbits

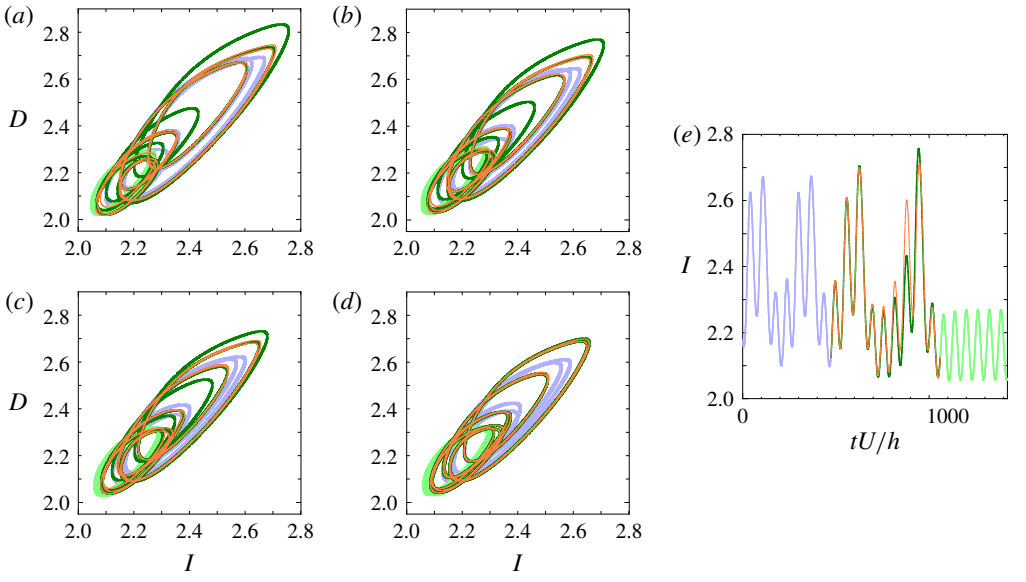

FIGURE 9. A pair of distinct heteroclinic orbits from the lower branch of P2 to the GPO that exhibit tangency in the (I, D)-projection. The light violet and light green lines represent the lower branch of P2 and the GPO, respectively. The green and orange lines correspond to the families of heteroclinic orbits. Starting from (*a*) the pair move closer to each other with decreasing Reynolds number until they merge to tangency at (*d*). The values of Reynolds number from (*a*) to (*d*) are: (*a*) $Re = 245$, (*b*) $Re = 242.5$, (*c*) $Re = 241.4$ and (*d*) $Re \approx 240.89$. The I of the two orbits as a function of time at $Re = 245$ is shown in (*e*). The green line is slightly thicker than the orange line in order to differentiate one heteroclinic orbit from the other, especially during the tangency. Thicker light green and light violet lines are used to differentiate the periodic orbits from the heteroclinic orbits.

from the lower branch of P2 to the GPO has actually been found to arise from the first heteroclinic tangency, i.e., tangent heteroclinic orbits, at $Re \approx 240.89$ (see figures 9 and 10).

6. Conclusion

We have reported the homoclinic tangency at $Re_T \approx 240.88$ with respect to the periodic edge state found by Kawahara & Kida (2001) in minimal plane Couette flow. To our knowledge, the identification of the first homoclinic tangency in this study is the earliest theoretical evidence of a boundary crisis leading to transient turbulence that eventually relaminarises. Although Riols *et al.* (2013) reported the presence of homoclinic tangle at the onset of chaotic dynamics in a Keplerian shear flow, they did not identify the onset as the tangency. We have confirmed that, as with the report by Grebogi *et al.* (1983) on the Hénon map, both the boundary crises at $Re_{cr1} \approx 240.46$ and $Re_{cr2} \approx 240.88$ are attributed to homoclinic tangencies at the two corresponding critical Reynolds numbers, which is probably the first such result for fluid flow systems. Even though the results here are for a minimal flow unit, the striking similarity of the boundary crisis on the periodic edge state found in this study to that on a streamwise-localised periodic edge state (Avila *et al.* 2013) as well as

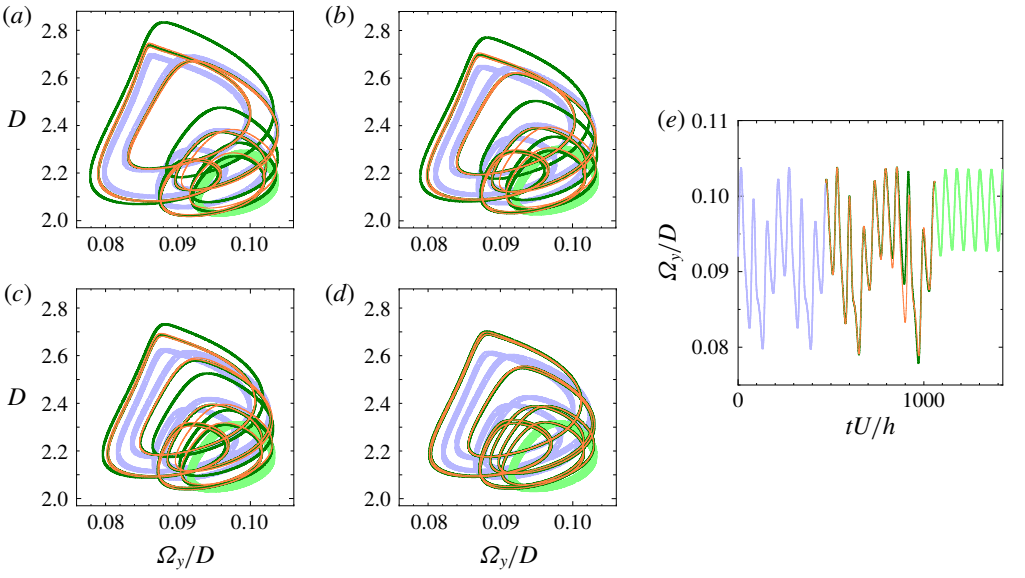

FIGURE 10. The same as figure 9 but for the $(\Omega_y/D, D)$-projection.

the recent investigation on the unstable manifold of the localised relative period orbit (Budanur & Hof 2017) in pipe flow encourage us to identify homoclinic tangency in pipe flow, if any, for the theoretical explanation of the onset of spatially localised transient turbulence – that is, a turbulent puff – in experiments.

Acknowledgements

This work has been partially supported by the Grant in Aid for Scientific Research (grant nos. 25249014, 26630055) from Japan Society for the Promotion of Science and the Basic Research Grant from University of the Philippines Los Baños (project code 14828). L.v.V. was supported by an NSERC Discovery Grant. J.R.T.L.'s doctoral study is supported by the Japanese government's MEXT scholarship (id no. 162100).

References

AVILA, M., MELLIBOVSKY, F., ROLAND, N. & HOF, B. 2013 Streamwise-localized solutions at the onset of turbulence in pipe flow. *Phys. Rev. Lett.* **110**, 224502.

BUDANUR, N. B. & HOF, B. 2017 Heteroclinic path to spatially localized chaos in pipe flow. *J. Fluid Mech.* **827**, R1.

CHIAN, A. C.-L., MUÑOZ, P. R. & REMPEL, E. L. 2013 Edge of chaos and genesis of turbulence. *Phys. Rev.* E **88**, 052910.

DOEDEL, E. J., KOOI, B. W., VAN VOORN, G. A. K. & KUZNETSOV, Y. A. 2009 Continuation of connecting orbits in 3D-ODEs (II): cycle-to-cycle connections. *Intl J. Bifurcation Chaos Appl. Sci. Eng.* **19**, 159–169.

ECKHARDT, B., FAISST, H., SCHMIEGEL, A. & SCHNEIDER, T. M. 2008 Dynamical systems and the transition to turbulence in linearly stable shear flows. *Phil. Trans. R. Soc. Lond.* A **366**, 1297–1315.

ECKHARDT, B., SCHNEIDER, T. M., HOF, B. & WESTERWEEL, J. 2007 Turbulence transition in pipe flow. *Annu. Rev. Fluid Mech.* **39**, 447–468.

GREBOGI, C., OTT, E. & YORKE, J. A. 1983 Crises, sudden changes in chaotic attractors, and transient chaos. *Physica* D **7**, 181–200.

GUCKENHEIMER, J. & HOLMES, P. 1983 *Nonlinear Oscillations, Dynamical Systems, and Bifurcations of Vector Fields*. Springer.

HAMILTON, J. M., KIM, J. & WALEFFE, F. 1995 Regeneration mechanisms of near-wall turbulence structures. *J. Fluid Mech.* **287**, 317–348.

ITANO, T. & TOH, S. 2001 The dynamics of bursting process in wall turbulence. *J. Phys. Soc. Japan* **70**, 703–716.

JIMÉNEZ, J., KAWAHARA, G., SIMENS, M. P., NAGATA, M. & SHIBA, M. 2005 Characterization of near-wall turbulence in terms of equilibrium and 'bursting' solutions. *Phys. Fluids* **17**, 015105.

JIMÉNEZ, J. & MOIN, P. 1991 The minimal flow unit in near-wall turbulence. *J. Fluid Mech.* **225**, 213–240.

KAWAHARA, G. 2005 Laminarization of minimal plane Couette flow: going beyond the basin of attraction of turbulence. *Phys. Fluids* **17**, 041702.

KAWAHARA, G. & KIDA, S. 2001 Periodic motion embedded in plane Couette turbulence: regeneration cycle and burst. *J. Fluid Mech.* **449**, 291–300.

KAWAHARA, G., UHLMANN, M. & VAN VEEN, L. 2012 The significance of simple invariant solutions in turbulent flows. *Annu. Rev. Fluid Mech.* **44**, 203–225.

KERSWELL, R. R. 2005 Recent progress in understanding the transition to turbulence in a pipe. *Nonlinearity* **18**, R17–44.

KIM, J., MOIN, P. & MOSER, R. D. 1987 Turbulence statistics in fully developed channel flow at low Reynolds number. *J. Fluid Mech.* **177**, 133–166.

KREILOS, T. & ECKHARDT, B. 2012 Periodic orbits near onset of chaos in plane Couette flow. *Chaos* **22**, 047505.

MCFADDEN, G. B., MURRAY, B. T. & BOISVERT, R. F. 1990 Elimination of spurious eigenvalues in the Chebyshev tau spectral method. *J. Comput. Phys.* **91**, 228–239.

MUÑOZ, P. R., BARROSO, J. J., CHIAN, A. C.-L. & REMPEL, E. L. 2012 Edge state and crisis in the Pierce diode. *Chaos* **22**, 033120.

NAGATA, M. 1990 Three-dimensional finite-amplitude solutions in plane Couette flow: bifurcation from infinity. *J. Fluid Mech.* **217**, 519–527.

OTT, E. 2002 *Chaos in Dynamical Systems*, 2nd edn. Cambridge University Press.

PALIS, J. & TAKENS, F. 1993 *Hyperbolicity and Sensitive Chaotic Dynamics at Homoclinic Bifurcations*. Cambridge University Press.

REYNOLDS, O. 1883 An experimental investigation of the circumstances which determine whether the motion of water shall be direct or sinuous, and of the law of resistance in parallel channels. *Phil. Trans. R. Soc.* **174**, 935–982.

RIOLS, A., RINCON, F., COSSU, C., LESUR, G., LONGARETTI, P.-Y., OGILVIE, G. I. & HERAULT, J. 2013 Global bifurcations to subcritical magnetorotational dynamo action in Keplerian shear flow. *J. Fluid Mech.* **731**, 1–45.

SÁNCHEZ, J., NET, M., GARCÍA-ARCHILLA, B. & SIMÓ, C. 2004 Newton–Krylov continuation of periodic orbits for Navier–Stokes flows. *J. Comput. Phys.* **201**, 13–33.

SCHNEIDER, T. M., GIBSON, J. F., LAGHA, M., DE LILLO, F. & ECKHARDT, B. 2008 Laminar-turbulent boundary in plane Couette flow. *Phys. Rev.* E **78**, 037301.

SHIMIZU, M., KAWAHARA, G., LUSTRO, J. R. T. & VAN VEEN, L. 2014 Route to chaos in minimal plane Couette flow. In *ECCOMAS Congress*, International Center for Numerical Methods in Engineering (CIMNE), Barcelona, Spain.

SKUFCA, J. D., YORKE, J. A. & ECKHARDT, B. 2006 Edge of chaos in a parallel shear flow. *Phys. Rev. Lett.* **96**, 174101.

VAN VEEN, L. & KAWAHARA, G. 2011 Homoclinic tangle on the edge of shear turbulence. *Phys. Rev. Lett.* **107**, 114501.

VAN VEEN, L., KAWAHARA, G. & MATSUMURA, A. 2011 On matrix-free computation of 2D unstable manifolds. *SIAM J. Sci. Comput.* **33**, 25–44.

VISWANATH, D. 2007 Recurrent motions within plane Couette turbulence. *J. Fluid Mech.* **580**, 339–358.

VOLLMER, J., SCHNEIDER, T. M. & ECKHARDT, B. 2009 Basin boundary, edge of chaos, and edge state in a two-dimensional model. *New J. Phys.* **11**, 1–23.